

On the Nature of ETG Turbulence and Cross-Scale Coupling

JENKO Frank

Max-Planck-Institut für Plasmaphysik,
EURATOM-Association, D-85748 Garching, Germany

(Received: 12 December 2003 / Accepted: 19 May 2004)

Abstract

Microturbulence in tokamaks and stellarators is studied via gyrokinetic simulation and semi-analytical theory. The focus is on electron temperature gradient (ETG) turbulence and its interactions with fluctuations at longer wavelengths. In this context, special attention is paid to the physics of edge transport barriers.

Keywords:

microturbulence, ETG mode, cross-scale coupling, transport barrier

1. Introduction

Plasma turbulence can be driven by a large number of microinstabilities, including ion temperature gradient (ITG) modes, trapped electron modes, electron drift waves, and electron temperature gradient (ETG) modes [1]. While the first three are associated with perpendicular spatial scales of roughly 1–50 ion gyroradii, ETG modes exist on smaller scales of typically 0.1–1 ion gyroradii. So far, almost all effort in computational and theoretical turbulence studies went into the investigation of isolated and (sometimes highly) idealized subsystems. However, with the advent of modern supercomputers, more comprehensive simulations become feasible, taking the multi-scale nature of the plasma turbulence problem seriously. In the present paper, the character of adiabatic ETG turbulence is reviewed, and the interactions of ETG turbulence with fluctuations at longer wavelengths are discussed. In this context, special attention is paid to the physics of edge transport barriers.

2. The character of adiabatic ETG turbulence

Neglecting Debye shielding effects, ETG and ITG modes are perfectly isomorphic in the electrostatic and adiabatic limit. Under these circumstances, it is therefore permissible to transfer linear results from the one to the other by simply interchanging the species labels. Consequently, the space and time scales of ETG modes are set by the electron gyroradius, ρ_e , and the inverse linear growth rate, L_{Te}/v_{te} . (As will become clear later in this Section, it is appropriate to use the temperature scale length L_{Te} as the reference scale, not the density scale length L_n or the minor/major radius of the torus.) However, even in the electrostatic and adiabatic limit, this ETG/ITG symmetry is broken in the nonlinear regime due to a subtle difference in the response of the adiabatic species

[2]. This is due to the zonal flow mode, characterized by fluctuations of the electrostatic potential with $k_y = k_{\parallel} = 0$, which does not participate in the parallel dynamics. Consequently, the electrons are never adiabatic for this mode and in the ITG case it must be subtracted out of the adiabatic term in the equation for the electrostatic potential [3]. By contrast, in the ETG case, the ions are made adiabatic by gyromotion, which affects every mode in the spectrum. So for adiabatic ETG turbulence the zonal flow mode is also adiabatic, forming the principal distinction between the two basic models.

2.1 High-amplitude streamers

The manifestation of this effect in nonlinear simulations is that while adiabatic ITG and ETG computations saturate at similar normalized levels in the sheared slab case (even consistent with mixing length expectations, $\chi \sim \gamma^{max}/k_{\perp}^2 \sim \rho^2 v_t/L_T$), toroidal ETG simulations can go to much higher amplitudes than their ITG counterparts [2]. When this is the case, they are characterized by a predominance of “streamer” modes, i.e., radially elongated vortices exhibiting the morphology shown in Fig. 4 of Ref. [2]. At the same time, the associated electron heat transport (which is always predominantly electrostatic, both with *and* without streamers [2,4]) is boosted by up to an order of magnitude or more with respect to mixing length expectations. Streamers have been observed both in tokamak [2,5,6] and in stellarator [4,7] geometry if and only if the underlying long-wavelength instabilities have a clear toroidal (as opposed to slab) character. For large aspect ratio tokamaks with circular cross section and small Shafranov shift, this is the case for $\hat{s} \geq 0.4$ and $R/L_{Te} \gg R/L_{Te}^{crit}$ [2]. Here, \hat{s} and R are, respectively, the magnetic shear and the major radius of the torus. Streamer

Corresponding author's e-mail: fsj@ipp.mpg.de

aspect ratios computed via the radial/poloidal anisotropy in the autocorrelation functions of $\tilde{\phi}$ are typically of the order of 2 [7]. This value seems somewhat low compared with the visual impression and indicates that refined measurements are called for; perhaps those inspired by percolation theory will prove useful. Nevertheless, we have found the following corollary to hold: if the correlation length ratio $\lambda_x/\lambda_y \gtrsim 2$ then streamers are predominant in the spatial morphology. For Cyclone Base Case parameters we find the dominant modes to arise near $k_y \rho_e = 0.15$ [2,6] and to exhibit a phase shift of $\sim \pi/3$ between $\tilde{\phi}$ and \tilde{T} , both results commensurate to the corresponding linear streamer [2]. An analysis of the transfer rates of $\mathbf{E} \times \mathbf{B}$ energy in the nonlinear saturated state [8] clearly confirms that streamers are driven predominantly by linear processes and that they may be viewed as residuals of linear modes. Nonlinear processes like modulational instabilities need not be invoked to explain streamer generation.

2.2 Secondary instabilities

Because of their similarity to the underlying linear modes, the nonlinear saturation of streamers can be interpreted in the framework of secondary instability theory. Depending on the importance of slab character of linear electrostatic ETG/ITG modes (as characterized by the intrinsic parallel velocity component), one finds that one of two distinct processes may dominate as nonlinear saturation mechanism [6]. Perpendicular shear in the *parallel* flow of the linear instability drives a (hereafter, ‘‘Cowley’’) secondary, described in detail in Ref. [9]. Importantly, this secondary is not sensitive to the form of the adiabatic response and thus leads to the same (mixing-length type) transport level in both slab cases. Predominantly curvature driven modes, on the other hand, are broken up by a (hereafter, ‘‘Rogers’’) secondary that is driven by the perpendicular shear in the eigenmode’s *perpendicular* $\mathbf{E} \times \mathbf{B}$ flow [2,5]. Due to the fact that the adiabatic ion response for the ETG case affects all modes, the Rogers secondary is significantly weakened on ρ_e scales, while on ion scales, it can access the zonal flow mode in $\tilde{\phi}$. Because $k_{\parallel} = 0$ for this mode, it is not affected by the adiabatic response and so remains free. This is the essential difference between the nonlinear dynamics of ETG and ITG modes. Consequently, for the toroidal case in which the Rogers secondary is more relevant, an ETG mode tends to saturate at a much higher normalized level than either its ITG counterpart or the corresponding mixing length expectations. With this enhancement, associated with the more resilient high-amplitude streamers, ETG-induced transport can, in principle, be comparable to electron energy transport induced by nonadiabatic ITG modes and trapped electron modes.

2.3 Zonal flows and fields

Zonal flows and fields are the $\mathbf{E} \times \mathbf{B}$ velocities and magnetic fields which result, respectively, from disturbances in $\tilde{\phi}$ and \tilde{A}_{\parallel} with a purely radial dependence ($k_x \neq 0$, $k_y = k_{\parallel} = 0$). (The latter can also be thought of as radial variations in

the q -profile.) They can be self-generated by the turbulence and may in turn act as its dominant nonlinear saturation mechanism [10]. There is much literature on this for ion scale turbulence, particularly ITG modes with adiabatic electrons [11,12] as well as edge turbulence [13,14], but much less is known about their behavior on electron gyroradius scales. For the stellarator simulation presented in Ref. [7], the time averaged root-mean-square (RMS) values of the $\mathbf{E} \times \mathbf{B}$ shearing rate, $\tilde{\Omega} \equiv \tilde{v}'_{E_y}$, and of the magnetic shear fluctuation, $\tilde{s} \equiv qR\tilde{B}'_y/B$, are given by $\tilde{\Omega}^{rms} \approx 0.12 v_{te}/R \sim 0.3 \gamma^{max}$ and $\tilde{s}^{rms} \approx 0.018$ where γ^{max} is the maximum linear growth rate. This is in stark contrast to results from ITG turbulence where $\tilde{\Omega}$ can significantly exceed γ^{max} (e.g., $\tilde{\Omega}^{max}/\gamma^{max} \sim 14$ in Ref. [15]). In the ITG case, one obtains the zonal flow saturation criterion $\tilde{\Omega}^{rms} \lesssim \gamma^{max}$ only after correcting for the ineffectiveness of the high frequency component of $\tilde{\Omega}$. Moreover, the zonal components of ETG turbulence contribute only 1 % or so to the total $\tilde{\phi}^{rms}$ [7]. This is again in contrast to the findings in the ITG case where zonal modes with $k_x \rho_i \sim 0.1$ tend to contribute significantly or even dominate the fluctuation free energy contained in $\tilde{\phi}$ (see, e.g., Ref. [15] and references therein). It is well known that low-amplitude ITG streamers are broken up by zonal flows. In the ETG case, however, the self-generated zonal flows are too weak (about 15–20 times weaker than in the ITG case as we have shown above) to break up the high-amplitude streamers. This finding is supported by recent theoretical investigations [16]. Moreover, since magnetic shear variations primarily affect the linear growth rates of the ETG modes driving the turbulence [17], a value of $\tilde{s}^{rms} \approx 0.018$ is certainly too small for zonal fields to play a significant role. Similar zonal flow/field saturation levels as the ones reported here have also been found in ETG simulations using tokamak geometry. Thus, we may conclude that, at least for a significant region in parameter space, zonal modes on ρ_e scales tend to play a subdominant role in the turbulent dynamics.

2.4 Semi-analytical transport estimate

Building on these results and insights, a simple numerical model with a universal fit parameter can be developed which was shown to agree fairly well with the results of nonlinear gyrokinetic computations [6]. The basic idea is to predict the saturation amplitude by balancing primary (γ_e) and secondary (γ_{nl}) growth rates. The latter are computed numerically by using high-amplitude ETG streamers as pseudo-equilibria. Since γ_{nl} is proportional to the amplitude of the primary mode in this regime, the saturation amplitude can thus be estimated. Furthermore, we take advantage of the fact that our computational results are all in the regime of strong turbulence, where $\chi_e \propto \tilde{\phi}$. This way we arrive at numerical transport estimates which exhibit reasonable agreement with the results from gyrokinetic computations [6]. Importantly, neither the linear growth rate nor the maximal value of $\gamma/\langle k_{\perp}^2 \rangle$ predicts the variation found in the nonlinear computations. Rather, it is the variation of the secondary growth rate as the linear eigenfunction changes

in response to the equilibrium parameters that correlates with the difference in the turbulent flux. The secondary growth rates exhibit a strong dependence on magnetic shear as the basic character changes from the Rogers (moderate positive shear) to Cowley (negative shear) type. The good agreement between the gyrokinetic computation and numerical model encourages us to pursue a semi-analytical treatment of the balance between long-wavelength primaries and secondaries, condensing several important pieces of information about the saturated nonlinear state into simple algebraic formulas. One finds that for $\hat{s} \gtrsim 0.4$ and $R/L_n \lesssim R/L_{Te} \gg R/L_{Te}^{crit}$ (algebraic expressions for R/L_{Te}^{crit} in tokamaks and the stellarator Wendelstein 7-AS have been derived in Refs. [18] and [4], respectively), transport by adiabatic, electrostatic ETG modes is approximately given by [8]

$$\chi_e = \frac{0.15}{\tau_e^{3/2} (1 + \hat{s}^2/2\hat{v})^2} \left(\frac{qR}{L_{Te}} \right)^3 \frac{\rho_e^2 v_{te}}{L_{Te}} \approx \mathcal{F}(q, \hat{s}, \tau_e) \frac{R}{L_{Te}} \frac{\rho_e^2 v_{te}}{L_{Te}}. \quad (1)$$

Here, $v = 0.53 q (k_y \rho_e) + \max\{0.09, 0.19 \hat{s}^2\} (q/\tau_e) (R/L_{Te}) (k_y \rho_e)^2$, $\hat{v} = v(k_y = k_y^d)$, $k_y^d = 4k_y^c/3$, $k_y^c \rho_e = \tau_e^{1/2} L_{Te} (qR)^{-1}$, and $\tau_e = T_e/T_i$. The agreement of this formula with fully nonlinear simulation results is surprisingly good. Note that another prediction of this semi-analytical model is that the poloidal length scale of the dominant modes is given by k_y^d . For Cyclone Base Case parameters (including $\hat{s} = 0.8$) we find $k_y^d \sim 0.13$, in good agreement to the results of nonlinear computations, which exhibit $k_y^d = 0.15 \pm 0.05$ [2,6]. An analogous treatment of adiabatic ITG turbulence leads to the estimate $\chi_i \approx \mathcal{G}(q, \hat{s}, \tau_e) (\rho_i^2 v_{ti}/L_{Ti})$ which is one order down in R/L_T compared to the ETG case, Eq. (1). A scaling like this has indeed been observed in nonlinear computations of adiabatic ITG turbulence [19,20]. Moreover, the model finding $\mathcal{G}(q = 1.4, \hat{s} = 0.8, \tau_i = 1) \sim 2$ is roughly consistent with the computational results which exhibit a prefactor of the order of 1.5. It should be kept in mind, however, that in contrast to the ETG case, adiabatic ITG turbulence can be controlled by zonal modes, especially near the linear threshold, an effect which is not accounted for by our model.

3. Interactions between ion and electron scale turbulence

Having shown that ETG-induced electron heat transport can be competitive with that from larger scale turbulence – caused, e.g., by nonadiabatic ITG modes, trapped electron modes, or electron drift waves – it is very interesting and important to study the nonlinear interactions between hyperfine-scale fluctuations at $k_\perp \rho_e \lesssim 1 \lesssim k_\perp \rho_i$ and fine-scale fluctuations at $k_\perp \rho_i \lesssim 1 \ll k_\perp L_T$. We certainly expect that the co-existence of these different types of turbulence cannot be characterized as a simple superposition. In general, there will be effects of the fine-scale turbulence on the hyperfine scales *and vice versa*. In the following, however, we will primarily assess how the ETG turbulence reacts to the presence of turbulent fluctuations at longer wavelengths.

3.1 Living in the tail of a cascade

Obviously, the hyperfine-scale turbulence “feels” both the quiescent background profiles and their modifications due to the fine-scale fluctuations. In order to better understand this effect, let us first discuss some basic properties of cascades in plasma microturbulence. The strong magnetic field lends the dynamics a quasi-two-dimensional character, such that parallels with two-dimensional Navier-Stokes turbulence can be drawn [21]. In the latter case, it is known that there exists a *dual* cascade: while energy is transferred to *larger* scales, enstrophy (i.e., mean-square vorticity, $\langle (\nabla \times v_E)^2 \rangle$) cascades to smaller scales [22]. Denoting the rate of the enstrophy cascade by ε , and the eddy size, lifetime, and velocity by ℓ , τ_ℓ , and v_ℓ , respectively, one can easily establish the following relations: $\varepsilon \sim (v_\ell/\ell)^2/\tau_\ell$, $\tau_\ell \sim \ell/v_\ell$, $k_\ell \sim 1/\ell$. From these one can derive Kraichnan’s famous energy spectrum of two-dimensional turbulence: $E(k_\ell) \propto \varepsilon^{2/3} k_\ell^{-3}$ [22]. Furthermore, for a nearly adiabatic plasma one obtains $\tilde{n}_\ell \propto \tilde{\phi}_\ell \propto \ell v_\ell \propto \varepsilon^{1/3} k_\ell^{-2}$. This result matches fairly well with nonlinear simulation results (see Ref. [7] and references therein) which yield exponents of the order of -2.3 . Another consequence is that the eddy turnover time τ_ℓ is independent of the eddy size ℓ . The same is true for the shearing rate associated with arbitrary (not necessarily zonal) $\mathbf{E} \times \mathbf{B}$ flows: $\tilde{\Omega} \propto k_\ell^2 \tilde{\phi}_\ell \sim \text{const}$. Assuming that zonal flows behave the same way, we expect that this result may be extended to purely radial fluctuations. And indeed, both gyrofluid simulations of adiabatic ITG turbulence [15] and two-scale gyrokinetic simulations of co-existing ITG/ETG turbulence [7] show that the zonal flow shearing rate is (almost) scale-independent. Thus, the comparison of the cascade properties in plasma microturbulence and in two-dimensional fluid turbulence seems to be helpful.

3.2 $\mathbf{E} \times \mathbf{B}$ shearing effects

To judge the importance of $\mathbf{E} \times \mathbf{B}$ shearing of hyperfine-scale eddies in the cascade induced by the fine-scale turbulence, three questions must be addressed. First, what is the amplitude/strength of these flows? It sets the value of $\tilde{\Omega}$. Second, what is the typical time scale of these flows with respect to that of the modes to be suppressed? It was shown in Ref. [15] that fast temporal variations of zonal $\mathbf{E} \times \mathbf{B}$ flows lead to a reduction of their shearing effectiveness. Of course, these two effects are interdependent, and the latter tends to weaken the effect of the former as the flow amplitude is increased. For ETG modes, this weakening is expected to be small due to time-scale separation. Third, what are the linear growth rates of the hyperfine-scale modes to be suppressed? As was shown in Sec. 2, in the case of ETG turbulence, the relevant linear growth rates are *not* the ones around the maximum of the k_y spectrum, but the ones near the long-wavelength cut-off. This certainly enhances the role of $\mathbf{E} \times \mathbf{B}$ shearing effects. In summary, for the shearing of hyperfine-scale eddies to be effective, $\tilde{\Omega}$ only has to exceed the linear ETG growth rates at long wavelengths. Whether zonal or non-zonal $\mathbf{E} \times \mathbf{B}$ flows dominate will depend largely on their

relative amplitude/strength.

3.3 Complex quasi-equilibria

Let us now focus on modifications of the equilibrium density and temperature profiles by the fine-scale turbulence. A rough estimate of τ_ℓ at long wavelengths is given by the maximum linear growth rate of the fine-scale modes. Since the latter is smaller than the respective quantity for ETG modes by the square root of the electron-to-ion mass ratio, the scale independence of τ_ℓ implies that the action of the larger scale fluctuations on the ETG turbulence may be regarded as slowly varying in time. On the other hand, the *spatial* structure of the resulting quasi-equilibria may be rather complex since the local gradients of density and temperature profiles need not be aligned with the radial direction. Nevertheless, the most important contributions come from relatively long wavelengths, such that there is a clear separation between quasi-equilibrium and fluctuation scales. This is because the gradients of the disturbances and of the background are known to be comparable at fine scales while the fluctuation spectra fall off (at least) like k_ℓ^{-2} [7]. The contributions of the fine-scale gradients to the total gradients therefore scale like k_ℓ^{-1} . This means that the effective electron heat diffusivity for ETG turbulence can be approximated by a weighted sum over the respective results for all possible quasi-equilibria. Since ETG turbulence often exhibits a superlinear increase of χ_e with R/L_{T_e} (or $\eta_e = L_n/L_{T_e}$ in the case of steep density profiles), background gradient fluctuations will lead to a (moderate) enhancement of the effective thermal diffusivity. Note that this effect is opposed to the one induced by $\mathbf{E} \times \mathbf{B}$ shearing.

3.4 Back-reaction on fine scales

So far, we have only discussed how the hyperfine scales are affected by the fine-scale turbulence. However, the hyperfine-scale turbulence may back-react on the fine scales via enhanced eddy damping (nonlocal energy transfer in k_ℓ space [23]) or other mechanisms. (Note that indirect back-reactions via zonal flows [24] may be judged unlikely, given the weak zonal flow excitation by ETG turbulence [7,16].) To address all of the above issues quantitatively requires comprehensive computations which treat the cross-scale interaction self-consistently. One such example will be discussed next.

3.5 Turbulence in an edge transport barrier

During the formation of an edge transport barrier, the turbulent transport within the barrier region is reduced by about an order of magnitude. This behavior is generally attributed to equilibrium $\mathbf{E} \times \mathbf{B}$ shear flows, although their precise origin remains unclear. If the corresponding $\mathbf{E} \times \mathbf{B}$ shearing rate reaches or exceeds the maximum growth rate of the fine-scale modes, the latter are suppressed. This raises questions about the role of hyperfine-scale turbulence in the H-mode edge. Due to their much smaller spatio-temporal scales, ETG modes are hardly affected by the above

mechanism and may provide a floor (at least) for the electron thermal transport. To investigate these issues, we have performed nonlinear gyrokinetic simulations with the `gene` code [2]. Equilibrium $\mathbf{E} \times \mathbf{B}$ flows have been included as prescribed, sinusoidal variations of v_{E_y} , with the amplitudes and wavelengths chosen in accordance with experimental findings (typical Mach numbers are in the range of 10 %, and $k_y \rho_i \gtrsim 0.1$). The other physical parameters were $R/L_n = 40$, $\eta_i = 2$, $\eta_e = 4$, $q = 2.4$, $\hat{s} = 0.8$, $\alpha = 0.5$, $T_i/T_e = 1$, and $1/\beta = m_i/m_e = 1836$. Magnetic fluctuations were taken into account (β and the normalized pressure gradient α were chosen consistently), and a \hat{s} - α geometry was employed. The time averaged k_y spectra of the electron thermal diffusivity χ_e for an L-mode case (no equilibrium flows) and an H-mode case (with equilibrium flows) are shown in Fig. 1. Therein, one can distinguish contributions from two regions in k_y space: (1) fine-scale fluctuations driven by electron drift waves (particle trapping is neglected; ITG modes are present but subdominant for the parameters used here), covering the range of $k_y \rho_i \lesssim 0.5$ with a peak around $k_y \rho_i \sim 0.2$; (2) hyperfine-scale turbulence at $k_y \rho_i > 0.5$ due to ETG modes, peaking around $k_y \rho_i \sim 1.5$. Although it might appear surprising at first that ETG modes can exist at these relatively long wavelengths, this finding is consistent with the semi-analytical theory presented in Sec. 2 when applied to a steep gradient regime. While in the L-mode case, the transport is clearly dominated by the fine scales (they contribute about 80 % to the total χ_e), the situation in the H-mode case is reversed (note that in this log-log plot, the density of modes increases with k_y). The total transport drops by almost one order of magnitude – an effect which can be attributed mostly to the suppression of the fine-scale turbulence, while the turbulent

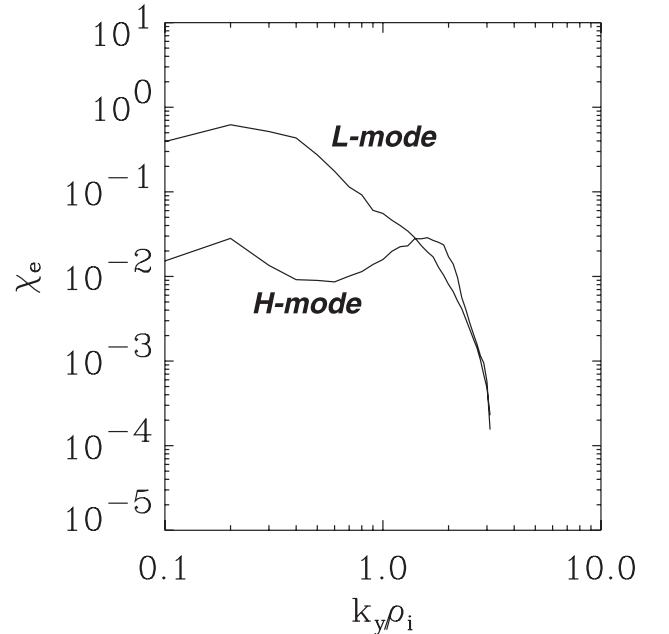


Fig. 1 Gyrokinetic simulations of L-mode and H-mode edge turbulence: time averaged k_y spectra of the electron thermal diffusivity χ_e .

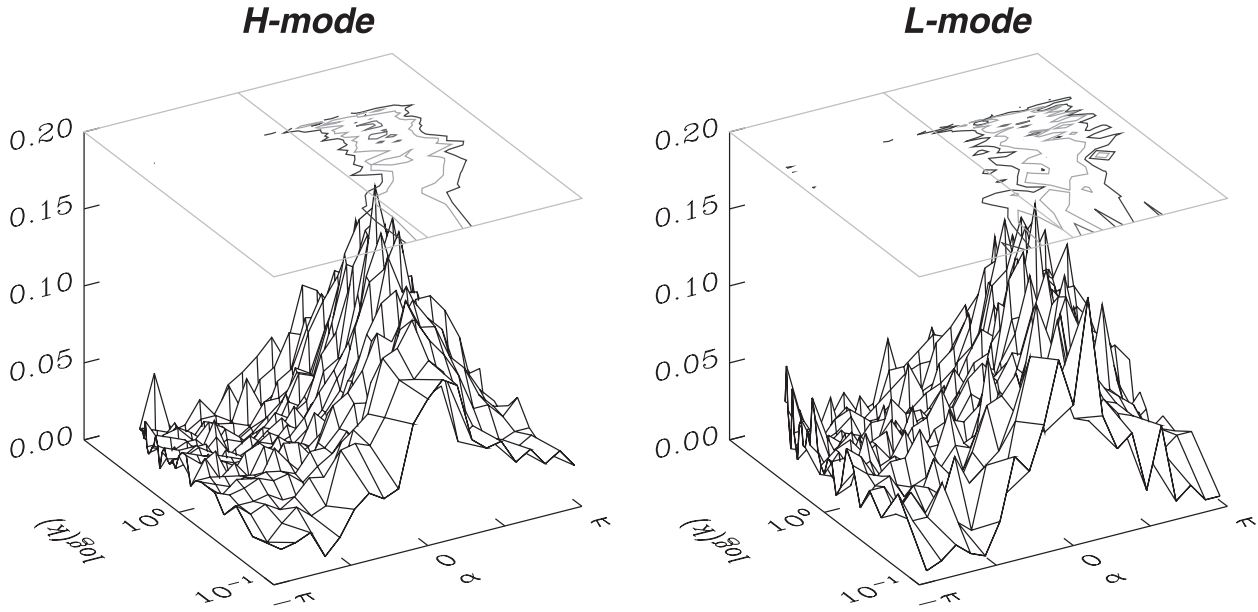


Fig. 2 Gyrokinetic simulations of L-mode and H-mode edge turbulence: phase shift between potential and electron temperature fluctuations as a function of k_y .

transport on hyperfine scales remains at L-mode levels. Nevertheless, one can observe a slight suppression of the high- k_y part of the spectrum in the presence of strong fine-scale dynamics. This is also reflected in the k_y spectra of the phase shifts between potential and electron temperature fluctuations shown in Fig. 2. Here, the L-mode case exhibits more ‘jitter’ at hyperfine scales than its H-mode counterpart, indicating that the nearly linear ETG modes are disturbed by the fine-scale turbulence. These results clearly show that cross-scale coupling mechanisms like the ones described above are active, invalidating a naive superposition approach. In particular, shearing by $\mathbf{E} \times \mathbf{B}$ flows seems to play an important role. More details and analyses of these computations will be published elsewhere.

3.6 Cross-scale coupling and bifurcations

It has been conjectured by S.-I. Itoh *et al.* [23,25] that cross-scale coupling mechanisms like the ones described above may lead to bifurcation transitions. E.g., the following scenario may be envisioned. Fine scales can suppress the hyperfine scales via $\mathbf{E} \times \mathbf{B}$ shearing if their amplitude is sufficiently large. On the other hand, strongly excited hyperfine scales can suppress the fine scales through enhanced eddy damping. This competition triggers bifurcations if the coupling strength between both ranges of scales exceeds a certain threshold. States in which one set of scales dominates the other can be shown to result. Moreover, equilibrium shear flows or other plasma parameters which influence the turbulence level can act as external control parameters. If such a scenario is indeed applicable to edge transport barriers is still under investigation. We note in passing that core transport barriers might also be subject to such transitions. Here, the role of electron drift waves would be played by trapped

electron modes or nonadiabatic ITG modes.

4. Summary

While for many years, plasma microturbulence research has been solely concerned with phenomena whose spatio-temporal scales are set by the ions, there is now a growing awareness that this limitation has to be overcome in search of more complete models of turbulent transport in fusion plasmas. Some recent developments along those lines are presented in this paper.

First, the physics of adiabatic ETG turbulence is reviewed. Due to a subtle difference in the adiabatic species’ response, the linear symmetry between ETG and ITG modes is nonlinearly broken. This leads to the emergence of radially elongated eddies (or streamers) with large fluctuation amplitudes in certain parameter regimes. These streamers are identified as residuals of linear modes, and their saturation level can be estimated by a semi-analytical theory based on the notion of secondary instabilities. Key features of the streamer-dominated turbulent state (first and foremost the associated electron heat diffusivity) may thus be predicted even quantitatively. An important finding is that ETG-induced transport is boosted by a factor of R/L_{Te} with respect to mixing length expectations.

Having shown that the hyperfine-scale dynamics can compete with that on fine scales, we discuss some dynamical coupling mechanisms between them. As expected, it is found that the co-existence of different types of turbulence cannot be characterized as a simple superposition. The ETG dynamics mainly perceives the fine-scale turbulence through $\mathbf{E} \times \mathbf{B}$ shearing and quasistatic modifications of the background equilibria. The hyperfine scales can in turn back-react on the longer wavelengths via enhanced eddy diffusivity

or other mechanisms. These generic findings and discussions prove useful for a deeper understanding of the physics of transport barriers. Here, both hyperfine-scale turbulence and nonlinear cross-scale coupling were observed to play a role. In particular, gyrokinetic simulations show that ETG turbulence provides a floor for H-mode edge transport. Whether the establishment of edge and/or core transport barriers involves a bifurcation from fine-scale to hyperfine-scale turbulence will be addressed in future investigations.

Acknowledgements

I would like to thank S.-I. Itoh and K. Itoh for stimulating discussions.

References

- [1] W. Horton, *Rev. Mod. Phys.* **71**, 735 (1999).
- [2] F. Jenko, W. Dorland, M. Kotschenreuther and B.N. Rogers, *Phys. Plasmas* **7**, 1904 (2000).
- [3] W. Dorland and G.W. Hammett, *Phys. Fluids B* **5**, 812 (1993).
- [4] F. Jenko and A. Kendl, *New Journal of Physics* **4**, 35 (2002).
- [5] W. Dorland, F. Jenko, M. Kotschenreuther and B.N. Rogers, *Phys. Rev. Lett.* **85**, 5579 (2000).
- [6] F. Jenko and W. Dorland, *Phys. Rev. Lett.* **89**, 225001 (2002).
- [7] F. Jenko and A. Kendl, *Phys. Plasmas* **9**, 4103 (2002).
- [8] F. Jenko, W. Dorland, B. Scott and D. Strintzi, *Theory of Fusion Plasmas* (SIF, Bologna, 2002), p. 157.
- [9] S.C. Cowley, R.M. Kulsrud and R. Sudan, *Phys. Fluids B* **3**, 2767 (1991).
- [10] P.H. Diamond and Y.B. Kim, *Phys. Fluids B* **3**, 1626 (1991).
- [11] Z. Lin, T.S. Hahm, W.W. Lee, W.M. Tang and R.B. White, *Science* **281**, 1835 (1998).
- [12] P.W. Terry, *Phys. Plasmas* **7**, 1653 (2000).
- [13] K. Hallatschek and D. Biskamp, *Phys. Rev. Lett.* **86**, 1223 (2001).
- [14] B. Scott, *Phys. Letters A* **320**, 53 (2003).
- [15] T.S. Hahm, M.A. Beer, Z. Lin, G.W. Hammett, W.W. Lee and W.M. Tang, *Phys. Plasmas* **6**, 922 (1999).
- [16] E. Kim, C. Holland and P.H. Diamond, *Phys. Rev. Lett.* **91**, 075003 (2003).
- [17] C. Holland and P.H. Diamond, *Phys. Plasmas* **9**, 3857 (2002).
- [18] F. Jenko, W. Dorland and G.W. Hammett, *Phys. Plasmas* **8**, 4096 (2001).
- [19] A.M. Dimits, G. Bateman, M.A. Beer *et al.*, *Phys. Plasmas* **7**, 969 (2000).
- [20] J. Candy and R.E. Waltz, *J. Comput. Phys.* **186**, 545 (2003).
- [21] A. Hasegawa and K. Mima, *Phys. Fluids* **21**, 87 (1978).
- [22] R.H. Kraichnan, *Phys. Fluids* **10**, 1417 (1967).
- [23] S.-I. Itoh and K. Itoh, *Plasma Phys. Control. Fusion* **43**, 1055 (2001).
- [24] J.Q. Li and Y. Kishimoto, *Phys. Rev. Lett.* **89**, 115002 (2002); *Phys. Plasmas* **10**, 683 (2003).
- [25] S.-I. Itoh, K. Itoh, M. Yagi *et al.*, *Phys. Plasmas* **9**, 1947 (2002).